Journal of Materials Chemistry A

ROYAL SOCIETY OF CHEMISTRY

PAPER

View Article Online
View Journal

Cite this: DOI: 10.1039/d5ta08055j

Water-stable direct air capture of CO_2 with microcapsules of task-specific ionic liquid and their electrothermal regeneration

Luma Al-Mahbobi,[a] Smita S. Dasari,[b] Aidan Klemm,[c] Harry M. Meyer III,[d] Yue Yuan,[d] Micah J. Green,[ab] Emily Pentzer *[ae] and Michelle K. Kidder *[c]

Received 1st October 2025
Accepted 22nd February 2026

DOI: 10.1039/d5ta08055j

rsc.li/materials-a

Microcapsules of the task specific ionic liquid (TSIL) 1-ethyl-3-methylimidazolium 2-cyanopyrrolide [EMIM][2CNpyr] with composite polydimethylsiloxane (PDMS) shells were fabricated for use in CO_2 direct air capture (DAC) conditions. The TSIL was encapsulated using an oil-in-oil emulsion as a templating procedure through two different approaches. In the first approach, a PDMS-polyurea (PU) shell was constructed by interfacial polymerization, while in the second approach, a graphene oxide (GO)-PDMS shell was constructed by cross-linking GO sheets. The composition and structure of both capsule types were fully characterized, and their CO_2 DAC performance was evaluated by gravimetric and breakthrough analysis. Both capsules exhibited competitive capacities, with the PDMS-PU capsules and the GO-PDMS capsules reaching 0.75 mol kg^{-1} and 0.66 mol kg^{-1}, respectively. We further demonstrate that both capsule systems can be regenerated with complementary electrothermal methods. Microwave (MW) regeneration was used for the PDMS-PU capsules, effectively releasing absorbed CO_2 in less than an hour. Owing to the electrical conductivity of GO, GO-PDMS capsules were regenerated *via* radio frequency heating (RF). This work highlights the importance and opportunity of tuning solid–liquid composite performance for advanced applications, including direct air capture of carbon dioxide.

Introduction

Levels of CO_2 in the atmosphere are rising primarily due to the combustion of fossil fuels. Despite advancements in renewable energy technologies in recent years, they are yet to overcome issues such as low energy density, land requirements, weather dependency, and safety concerns. Although it is imperative to control the rate of emission of CO_2 and other greenhouse gases, traditional reliance on natural CO_2 sinks, such as forests and oceans, is not sufficient to reach net-zero emissions. Carbon capture is required not only for flue gas separation,[1,2] but also direct air capture (DAC),[3] in order to lower the CO_2 concentration in ambient air, the latter of which is the more challenging and critical approach.[4]

Materials for both point source and DAC have been developed, studied, and deployed at commercial scale with both liquid and solid state systems being extensively studied.[5] Amine scrubbing is the dominant CO_2 separation technology for flue gas, typically absorbing CO_2 at 5–15% concentrations.[6] However, under ambient CO_2 concentrations (*ca.* >0.04%), their use becomes impractical, both in terms of cost and long-term solvent stability, making it difficult for aqueous amines to efficiently capture CO_2 without excessive energy input due to the high heat capacity of water.[7] Further, aqueous amines have high regeneration energy requirements, can undergo oxidative degradation, and are corrosive, further making them unfavorable for DAC.

In contrast to aqueous amines, hydroxide solutions and ionic liquids (ILs) have shown promise for DAC applications. Aqueous hydroxides have a strong affinity to CO_2, forming carbonates; however, regenerating temperatures, up to 900 °C are required, which is energy intensive, among other concerns including high corrosivity.[8] On the other hand, ILs are an emerging class of liquids for CO_2 and are characterized by low volatility, high thermal stability, and have tuneability for solvating environments. Thus, ILs are attractive solvents for DAC applications[9,10] not only for their ability to chemisorb CO_2, but also to physisorb it into high free volume arising from the poor packing of ions.[11–14] Recently, imidazolium-based ILs have been modified to increase affinity for CO_2 by changing the identity of the anion or cation, or by incorporating amine groups to enable chemisorption with CO_2.[15–18] Such task-specific

[a]Department of Materials Science and Engineering, Texas A&M University, College Station, Texas 77843, USA. E-mail: emilypentzer@tamu.edu
[b]Artie McFerrin Department of Chemical Engineering, Texas A&M University, College Station, Texas 77843, USA
[c]Energy Science and Technology Directorate, Oak Ridge National Laboratory, Oak Ridge, Tennessee 37831, USA. E-mail: kidderm@ornl.gov
[d]Physical Sciences Directorate, Oak Ridge National Laboratory, Oak Ridge, Tennessee 37831, USA
[e]Department of Chemistry, Texas A&M University, College Station, Texas 77843, USA

ILs (TSILs) exhibit competitive capacities among emerging DAC materials. However, when TSILs bind to CO_2, their molecular mobility is restricted, leading to increased viscosity. The higher viscosities slow the movement of CO_2 into the sorbent, causing mass transport limitations.[16] This challenge is similar to what is observed in traditional liquid amine systems, where high viscosity and low diffusivity lead to slow kinetics and reduced sorption efficiency.[19]

A class of commercially deployed DAC sorbents that overcome diffusion limitations and viscosity issues include amine-modified solids. Amine-modified solids are based on highly porous structures, such as silicas,[20,21] alumina,[20] and carbon-based materials,[22] which are impregnated or chemically functionalized to bear free amine groups. Combining the chemical reactivity of amine groups and the high surface area of the support yields preferable conditions for DAC (*i.e.*, low CO_2 concentration) by mitigating diffusion constraints inherent to bulk liquid sorbents.[23] Further, these materials are relatively inexpensive and can be readily scaled and recycled.[24] A major limitation to amine-modified porous solids is that they suffer degradation during thermal cycling, which increases costs due to the need for consistent supply, removal, and replacement. Other porous structures being investigated for DAC are metal–organic frameworks (MOFs),[25] crystalline structures composed of metal ions coordinated with organic linkers. MOFs have been modified with amines, much like porous silica, which has significantly increased sorption performance.[26] While promising, the commercial feasibility remains limited due to complex synthesis for scalability, poor stability under humid and acidic conditions, or exposure to high temperatures which can induce degradation.

Solid–liquid composites, such as liquid-filled microcapsules, have recently emerged as a promising class of materials for DAC. Microencapsulation offers a variety of advantages, most relevant to DAC are increased contact surface area, mitigation of viscosity diffusion barriers, ease of handling, overcome mass transport and diffusivity issues, and tunability for selectivity. Hydroxides, amines, ILs, and TSILs have all been encapsulated for CO_2 capture applications, leading to increased uptake rates compare to the bulk liquid.[27–29] Encapsulation methods include the use of microfluidics,[30,31] phase inversion,[32] and a soft-template approach, the latter of which approach offers a flexible and scalable route for tailoring compositions.[33–35] We have has previously reported the encapsulation of ILs using a soft template approach in a nonaqueous Pickering-emulsion with interfacial polymerization of a diamine and diisocyanate, forming a polyurea shell.[36–38] The encapsulation in a graphene oxide-polyurea (GO-PU) shells of generic ILs leads to faster CO_2 saturation due to increased surface area.[37,39] Further, the capture performance of TSILs encapsulated in the same GO-PU shell has demonstrated fast absorption rates and stable performance over multiple cycles under low CO_2 concentrations (500–5000 ppm) and varying humidity levels.[40,41] We have also demonstrated that ILs and amines mixtures encapsulated in GO-PU shell have higher thermal stability over multiple cycles compared to the bulk liquid; however, under DAC conditions, the capacities of these capsules suffer due to limited CO_2 diffusion.[29] Recently, we investigated alternative shell materials such as CO_2-derived polycarbonate.[42] In this approach, ILs were encapsulated in a double-emulsion soft-template, utilizing modified silica surfactant particles.[38] These capsules showed increased CO_2 uptake rates and eliminated core contamination, the latter being an issue for interfacial polymerization encapsulation. These works demonstrate the versatility of soft-template encapsulation for reactive cores. Although the performance of encapsuled ILs, TSILs, and amines is promising, the core–shell structures are yet to accommodate the ultra-low CO_2 partial pressure in the atmosphere.

To target DAC applications, microcapsules must meet the critical criteria of high capacity, selectivity, kinetics for sorption, low regeneration energy requirement, and high cyclability. This can be achieved by modifying the shell, aiming to tune the structures to enhance both permeability and selectivity by incorporating CO_2-philic functional groups, such as amines, and utilizing permeable polymers like polydimethylsiloxane (PDMS). The flexible nature of the PDMS backbone plays a significant role in permeability, making it attractive for gas separation membranes.[43–46] Indeed, PDMS has shown promise as a shell material in aqueous hydroxide microcapsules, formed by a microfluidic technique, due to its thermal stability and CO_2-permeability,[27] but the approach is less applicable to viscous liquids such as TSILs. Encapsulating TSILs within PDMS shells offers the potential to create modular, reusable, and high-performance materials for widespread use in carbon capture. We propose that the unique attributes of ILs and PDMS can be used to overcome existing technical barriers and contribute to the development of scalable DAC solutions.

Although tailoring the liquid core and polymer shell can enhance capacity and selectivity, a critical challenge is low and efficient energy methods for regeneration; hence, alternative regeneration approaches for carbon capture materials are emerging of urgent interest. Many regeneration techniques have been explored including convection heating,[47] pressure swing,[48] moisture swing,[49] vacuum swing,[50] and the use of chemical regeneration.[51] Recently electrothermal heating, more specifically microwave heating (MW), has emerged as a favorable low energy approach for regeneration of carbon capture materials due to its ability to induce localized heating, presenting a significant improvement in regeneration efficiency compared to conventional convection heating.[10,52–54] Another alternative method of electrothermal regeneration is radio frequency (RF) which is widely used in commercial applications, such as food processing,[55] textile drying, and sterilization,[56] medical treatments, and others, yet underexplored for CO_2 sorbent regeneration.[57,58] The development of innovative energy-efficient regeneration techniques is vital to improve the scalability and viability of CO_2 capture systems.

Herein, we report the production of microcapsules containing a core liquid and PDMS composite shell for carbon capture, the performance in carbon capture under DAC conditions, and the ability to use MW and RF induced heating to reach temperatures for regeneration. The TSIL 1-ethyl-3-methylimidazolium 2-cyanopyrrolide ([EMIM][2CNpyr]) was chosen as the core liquid due to its high CO_2 capacity (5 mol

kg^{-1} at 1 bar CO_2), its low temperature required for thermal regeneration (~55 °C), and its polarity which should allow for MW and/or RF active regeneration. Microcapsules were fabricated with PDMS-based composite shells using two oil-in-oil emulsion-templated approaches. In the first, the TSIL was encapsulated *via* interfacial polymerization of a diamine and diisocyanate to form a polyurea shell, with PDMS serving as a surfactant. In the second, a reactive, modified graphene oxide surfactant was cross-linked with different PDMS polymers. These approaches were designed to target distinct electrothermal heating modalities, MW heating for PDMS-PU and RF regeneration for GO-PDMS, enabling assessment of both modes and providing insight into their practical feasibility and tunability for scalable DAC systems. The characterized microcapsules' performance was evaluated under pure and 410 ppm CO_2 concentrations for up to 12 cycles, maintaining 76 and 82% of their initial capacities for PDMS-PU and GO-PDMS composites, respectively. Further, their electrothermal regeneration with both MW and RF was investigated. Additionally, their performance stability after soaking in water was investigated. This research demonstrates both the potential of utilizing microcapsules for DAC applications, as well as the applicability of electrothermal heating as a potential low-energy regeneration approach.

Experimental

Materials

Graphite flakes, potassium permanganate ($KMnO_4$), hexamethylene diisocyanate (HDI), ethylene diamine (EDA), poly(-dimethylsiloxane), bis(3-aminopropyl) terminated (DA-PDMS), poly(dimethylsiloxane) diglycidyl ether terminated (DGEP), polyethyleneimine (branched, average Mw ~800) (PEI), isopropanol (IPA), hexanes, toluene, butylamine, EMIM-Br, methanol, Amberlite IRN78 hydroxide (AER) form, and 2-cyanopyrole were purchased from Sigma Aldrich. Octane was purchased from Oakwood Chemical. Hydrogen peroxide (H_2O_2) in water (30%) was purchased from Fisher Scientific. Sulfuric acid (H_2SO_4), *N*,*N*-dimethylformamide (DMF), and 1-octadecylamine (97%) were purchased from Alfa Aesar. (3–5% aminoethylaminoisobutylmethylsiloxane)-dimethylsiloxane copolymer (AMS) was purchased from Gelest. 1-Butyl-3-methylimidazolium tetrafluoroborate ([BMIM][BF_4], 99%) was purchased from Iolitec.

MGO synthesis

Graphene oxide (GO) was synthesized following a modified Hummers' method based on a previously reported procedure.[37] Briefly, 133 mL of H_2SO_4 was gradually added to 1 g of graphite flakes and the mixture was stirred at 300 rpm. Then, 4 g of $KMnO_4$ was gradually added to the solution at a rate of 1 g per day while stirring continued. The reaction was quenched with ice water and 30% H_2O_2 was added dropwise until the solution changed color from burgundy to brown. The precipitated GO sheets were thoroughly washed with IPA until the pH of the supernatant was neutral, then dried under vacuum overnight.

After drying, 100 mg of GO sheets were weighed and dispersed in 50 mL of DMF under sonication, followed by heating to 55 °C while stirring. To this reaction mixture, 100 mg of octadecylamine dissolved in 50 mL of toluene was added and allowed to react for 15 minutes to facilitate alkylation and interlayer spacing. Then 1.2 mL of DA-PDMS in toluene was added to the flask and allowed to react for 1 hour. The resulting MGO sheets were then washed several times with toluene, dried under vacuum, ground, then dispersed in octane at a concentration of 10 mg mL^{-1} for use as a surfactant in GO-PDMS capsules. Their functionalization was confirmed by Fourier transform infrared (FTIR) spectroscopy, performed using a Thermo Fischer iS50, equipped with a diamond ATR and DLaTGS detector, for 32 scans at resolution 4 cm^{-1}, and by X-ray Photoelectron Spectroscopy (XPS) performed using a Thermo Scientific (Waltham, MA, USA) Model K-Alpha instrument, utilizing monochromated, microfocused, Al K_α X-rays (1486.6 eV) with a variable spot size (30–400 μm). A 400 μm X-ray spot was used for the maximum signal and to obtain an average surface composition over the largest possible area. The instrument had a hemispherical electron energy analyzer equipped with a 128-channel detector system. Base pressure in the analysis chamber was typically 2×10^{-9} mbar or lower. The powders were prepared for analysis by dispersing materials onto double-sided tape on clean glass slides. Sufficient material was used to prevent any interference signals from the tape. Next, high-resolution core level spectra (step size 0.1 eV, pass energy 50 eV) were acquired for a detailed chemical state analysis. C KLL (Auger) spectra were recorded using a step size of 2 eV and a pass energy of 100 eV. All spectra were acquired with the charge neutralization flood gun (combination of low energy electrons and argon ions) turned on to maintain stable analysis condition. A typical pressure in the analysis chamber with the flood gun operating was 2×10^{-7} mbar. Data were collected and processed using the Thermo Scientific Avantage XPS software package (v.5.96).

[EMIM][2CNpyr] synthesis

20 g of AER was weighed and slurried with methanol. This slurry was poured into a 3/4 in diameter × 25 in column with a quartz wool plug. The column was allowed to equilibrate for 30 min. 2.0 grams of [EMIM][Br] was dissolved in *ca.* 2 mL of methanol. This was placed carefully on top of the AER column, *ca.* 150 mL of methanol used to elute the column with a steady drip over *ca.* 15 min into a 300 mL round bottom flask. The methanol was reduced *via* rotovap to *ca.* 50 mL. An equimolar amount of 2-cyanopyrole was added to the methanol solution of [EMIM][OH]. This was stirred at room temperature for overnight. The methanol and water formed was removed *via* rotovap at 40–50 °C and held for *ca.* 4 h. The absence of residual bromide in the [EMIM][OH] intermediate was confirmed by (0.171 N) silver nitrate test where no visible white or yellowish silver(I) bromide precipitate was observed. The removal of residual moisture was carried out under vacuum at 70 °C overnight. The molecular structure of [EMIM][2-CNpyr] was confirmed by ^{1}H-NMR on a 60 MHz Nanalysis.

PDMS-PU capsules synthesis

To an 8 mL vial, 200 μL of [EMIM][2CNpyr] was added and mixed with EDA (0.7 mmol). To that vial, the immiscible phase consisting of AMS polymer (100 μL) in 1 mL of octane was added to the vial and emulsified under 30 000 rpm for 30 seconds using a VWR 200 Homogenizer. The emulsion was diluted with octane then 1 mmol of HDI in octane was added dropwise to the emulsion and left to polymerize at the interface with EDA and the amine functionalities on AMS for 2 hours. The formed capsules were then quenched with butylamine, washed with octane and hexanes, and dried under vacuum over night for characterization. The capsules were initially evaluated by optical microscopy imaging using a Motic SMZ-171 microscope. Further, the capsules morphology was investigated by imaging with scanning electron microscopy (Zeiss Merlin FE-SEM), and their cross-section obtained by a Hitachi NB5000 FIB/SEM (Hitachi High Technologies Corporation, Japan) milling operated at 40 kV, followed by a reduction to 5 kV for imaging. The capsules size was determined by a Partica LA-960S Laser Diffraction Particle Size Analyzer.

GO-PDMS capsules synthesis

Pristine [EMIM][2CNpyr] (200 μL) was added to a vial and 1 mL of MGO in octane (10 mg mL^{-1}) was added to the vial and emulsified under 30 000 rpm for 1 minute. The emulsion was diluted with octane then DGEP (100 μL) diluted in octane was added dropwise to the emulsion and left to react with the remaining primary amine functionalities on the MGO for 15 min at 55 °C. The emulsion was washed with octane and AMS copolymer (200 μL) in octane was added and left to react with the remaining unreacted epoxide functionalities for 15 min at 55 °C. Finally, the grafted AMS polymer was crosslinked with HDI (0.6 mmol) for 1 hour and quenched with butylamine before washing and drying under vacuum over night for characterization.

Core weight loading analysis

The IL content in the capsules was determined using ^{1}H NMR spectroscopy. For this, 20 mg of capsules were mixed with 1 mL of a 0.039 M mesitylene solution in DMSO-d_6, serving as an internal standard. The mixture was analyzed using a Bruker Ascend III HD 500 MHz NMR Magnet, and the weight percentage of IL was calculated based on the relative integration of the IL and mesitylene signals (see Table S2 for more details). Additionally, gravimetric analysis was performed to verify the IL weight loading in the capsules. Capsules were weighed before and after core extraction, where the IL was removed using DMSO. The difference in mass provided a measurement of the core weight loading (Table S2).

Gravimetric CO_2 sorption

CO_2 sorption and desorption at pure and 410 ppm CO_2 were performed using a thermogravimetric TA Instruments Discovery TGA 5500. The sample mass was first stabilized under N_2 (25 mL min^{-1} flow rate) at 65 °C for 1 hour to remove volatiles & absorbed CO_2. The desorption temperature of 65 °C was selected based on preliminary temperature-screening experiments to ensure complete and rapid CO_2 release from the encapsulated TSIL while avoiding thermal degradation. Once a baseline was obtained, the sample was allowed to cool to 30 °C and then CO_2 was introduced (either pure or 410 ppm balanced by N_2, 25 mL min^{-1} flow rate), and sorption was monitored until equilibrium was reached, denoted by a plateau in weight gain. Desorption was then carried out by switching back to N_2 and heating to 65 °C for 25 minutes, the minimum temperature observed for complete CO_2 release. The cycle was repeated after re-stabilizing the baseline and cooling to 30 °C. Cyclic sorption-desorption experiments were conducted over 12 consecutive cycles under identical operating conditions to evaluate the short-term repeatability of CO_2 uptake and release and to establish preliminary evidence of stable regeneration behavior for the capsule materials.

Breakthrough experiments & MW regeneration

The capsules were dried under vacuum at 65 °C, and cooled to 25 °C under argon (Ar). Breakthrough experiments for DAC were conducted using 300 ± 50 mg of the dried capsules carefully packed into a 0.305″ PTFE column (Kidder, M. K., Klemm, A.; US Patent Application 19/287 907, 2026). 410 ppm CO_2 balanced by N_2 gas was fed at 180 sccm, first through a bypass for calibrating an infrared LI-850 CO_2/H_2O gas analyzer, then through the sample column. The effluent CO_2 concentration was recorded until it matched the feed concentration, indicating saturation. CO_2 capacity was determined by integrating the breakthrough curve using eqn (1).

$$z = \frac{\int_0^t (C_0 - C)\mathrm{d}t \times F}{W \times \hat{V}_{\mathrm{STP}}} \quad (1)$$

where z is the CO_2 loading in mol kg^{-1} of sorbent. C_0 is the dimensionless feed CO_2 composition (concentration in ppm × 10^6), C is the dimensionless effluent CO_2 composition (concentration in ppm × 10^6), t is time in minutes, F is the total mass flowrate of the feed gas in sccm, W is the weight of the sample, and $\hat{V}_{\mathrm{STP}}$ is the molar volume of CO_2 at STP (22.4 scc CO_2/mmol CO_2, assuming ideal gas law in dilute conditions). Breakthrough time (t_{BT}) and pseudoequilibrium time (t_{PE}) were defined as the times when effluent CO_2 reached 5% and 95% of the feed concentration, respectively.

For microwave heating desorption, the capsule-packed column was placed inside a CEM Discover 2.0; 2.45 GHz, 1–300 W microwave chamber. The sorbent temperature was controlled at 65 °C (±3 °C) using the instrument's contactless infrared temperature sensor, which measures the temperature of the microwave-heated sample through the PTFE sample packed column and regulates the applied continuous microwave power (5 W) *via* closed-loop feedback. This measurement provides a representative bulk temperature for temperature control during desorption; however, it does not yield spatially resolved temperature distributions within the packed sorbent bed. The desorbed CO_2 was carried by a nitrogen flow (180

sccm) and monitored using the LI-850 IR CO_2 analyzer connected to the column outlet.

RF heating

A signal generator (Rigol Inc., DSG815) and an RF amplifier (ZHL-100 W-GAN + MiniCircuits) were used to supply RF power to a fringing-field applicator *via* a 50 Ohm coaxial cable. The RF applicator was custom made from PCB Power Inc. The applicator has a heating zone of ~1 cm and is made of copper traces drawn on a KAPPA 438 substrate. A FLIR A655sc thermal camera was used to safely measure the maximum temperature of the sample when heated *via* RF. The entire RF setup is placed inside a Faraday cage made out of brass mesh.

RF frequency sweep. RF-induced heating rates were measured in 1 MHz intervals from 1–200 MHz using 1.6 W of applied power. This was achieved by programming a stepwise heat-cool frequency sweep into the signal generator. Each sample was heated for 1 s and then cooled for 13 s before advancing to the next 1 MHz incremental step.[59] The heating rates for each frequency were calculated by analyzing the slope of the initial linear region in the temperature *vs.* time plots.

Regeneration of CO_2. The capsules before and after CO_2 absorption were heated for 30 minutes at a temperature of ~65 °C, by modulating the applied power between 1 to 2 W. The frequency was maintained constant for these experiments (128 MHz for CO_2 loaded capsules & 140 MHz for lean capsules).

Vector network analysis. A vector network analyzer (VNA) (SVA1015X, Siglent Technologies) was used to find the reflection coefficient (S_{11}) characteristics of the bare applicator, and the different lean & CO_2 loaded capsules. The samples (sample under test) were placed on the applicator, which was connected to PORT 1 using a 50 ohm coaxial cable. Based on previous work, the frequency at which the lowest S_{11} value is observed, is the best frequency for RF heating.[60]

Results and discussion

Microcapsules with a core of the TSIL [EMIM][2CNpyr] and PDMS-based composite shells were prepared using a non-aqueous emulsion as template (*i.e.*, droplets of the TSIL in a continuous octane phase). Briefly, PDMS-PU capsules were formulated by interfacial polymerization between ethylene diamine (EDA) and hexamethylene diisocyanate (HDI), while using aminoethylaminoisobutylmethylsiloxane-dimethylsiloxane co-polymer (AMS) as a surfactant (Scheme 1A). Alternatively, GO-PDMS capsules were prepared by cross-linking an alkyl chain-PDMS-modified graphene oxide (MGO), which served as surfactant, at the surface of the emulsion droplets. Here, the primary amines on MGO were reacted with epoxide groups from excess diglycidyl ether terminated PDMS

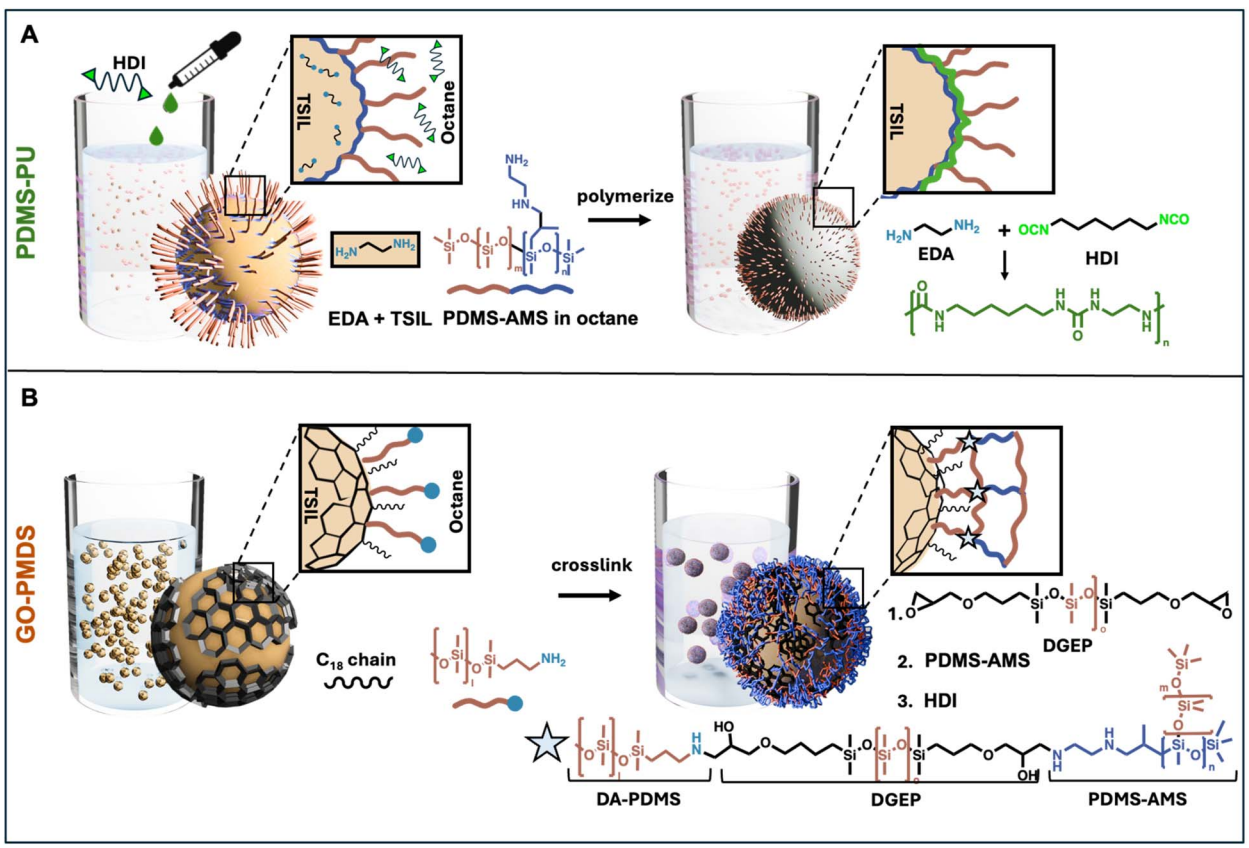

Scheme 1 Schematic showing formulation of microcapsules with core of the TSIL [EMIM][2CNpyr] and shells of (A) PDMS-PU, and (B) GO-PDMS.

(DGEP) for 1 hour. The emulsion was washed, then AMS was added to react with the remaining epoxide groups grafted on MGO to grow the shell. Lastly, HDI was added to the continuous phase to enhance shell cross-linking and quench any residual amines (Scheme 1B).

Optical microscopy images of PDMS-PU capsules in suspension are shown in Fig. S1A and images of the isolated capsules are shown in Fig. S1B and C, whereas images of GO-PDMS capsules are shown Fig. S2. The liquid content of the capsules was qualitatively confirmed by a "squish test", where the capsules are compressed between 2 glass slides and imaged (Fig. S1D for PDMS-PU capsules and Fig. S2D for GO-PDMS capsules). Both sets of capsules were dried under reduced pressure before further characterization. The loading of the liquid core was quantitatively determined gravimetrically by weighing the capsules before and after liquid extraction, and by ^{1}H NMR, 500 MHz, revealing capsules are ~50 wt% of the liquid core.

Morphology and structure

The morphology of the microcapsules was revealed by scanning electron microscopy (SEM), as shown in Fig. 1A for PDMS-PU microcapsules. These PDMS-PU microcapsules were spherical and had a relatively smooth surface. This supports that polymerization occurred uniformly at the interface of the emulsion droplet (Fig. 1B and C). The SEM-FIB cross-section of these PDMS-PU capsules (Fig. 1B inset) supports a core–shell structure, as expected from the interfacial polymerization synthesis. Particle size, as determined by laser diffraction, shows a Gaussian distribution of the particle diameter of PDMS-PU microcapsules with a median value of 6 ± 4 μm (Fig. 1D).

GO-PDMS microcapsules were significantly larger and had a more textured surface (Fig. 1E–G) compared to the PDMS-PU capsules. The surface roughness may be attributed to the presence of nanosheets. GO-PDMS capsules also have a narrower size distribution than PDMS-PU capsules, with a median diameter of 35 ± 21 μm (Fig. 1H). The difference in size distribution may be the result from differences in interfacial forces and stabilization mechanisms provided by each type of surfactant. For PDMS-PU, the relatively low molecular weight polymeric surfactant reduces the interfacial tension by diffusing rapidly to the interface, allowing for stabilization of smaller droplets during emulsification. Alternatively, for GO-PDMS the polymer-modified nanosheets may diffuse to the interface more slowly, and thus smaller droplets coalesce before surfactant can stabilize them. Notably, the GO-PDMS capsules have a similar size distributions to those previously prepared from alkylated GO stabilized emulsions, indicating a distinction for soft templating in particle stabilized emulsions (*e.g.*, Pickering emulsions).[29]

The FTIR spectra of the capsules and their constituents are shown in Fig. 2A. FTIR was used to aid in confirming the alkylation and PDMS grafting on the GO (see Fig. S3 for comparison of MGO and its components). The FTIR spectrum of the PDMS-PU capsules confirms the presence of both the core and shell materials. The characteristic peak of the cyano group at 2180 cm^{-1} verifies the presence of the TSIL [EMIM][2CNpyr] and the characteristic stretching frequencies at Si–O at 1013 cm^{-1} and Si–CH_3 at 1258 cm^{-1}, indicate successful incorporation of PDMS. The pronounced peak at 3320 cm^{-1} is attributed N–H stretching, which is present in both the polyurea and TSIL. The spectrum of the GO-PDMS capsules similarly confirms the presence of the TSIL; the slight shift of the cyano peak to 2210 cm^{-1} is attributed to CO_2 binding.[61] The characteristic peaks of PDMS are present, and the presence of MGO is supported by the broader N–H stretching at 3320 cm^{-1} is attributed to the crosslinked AMS polymer. These results confirm the successful integration of the core and shell materials in both capsule systems.

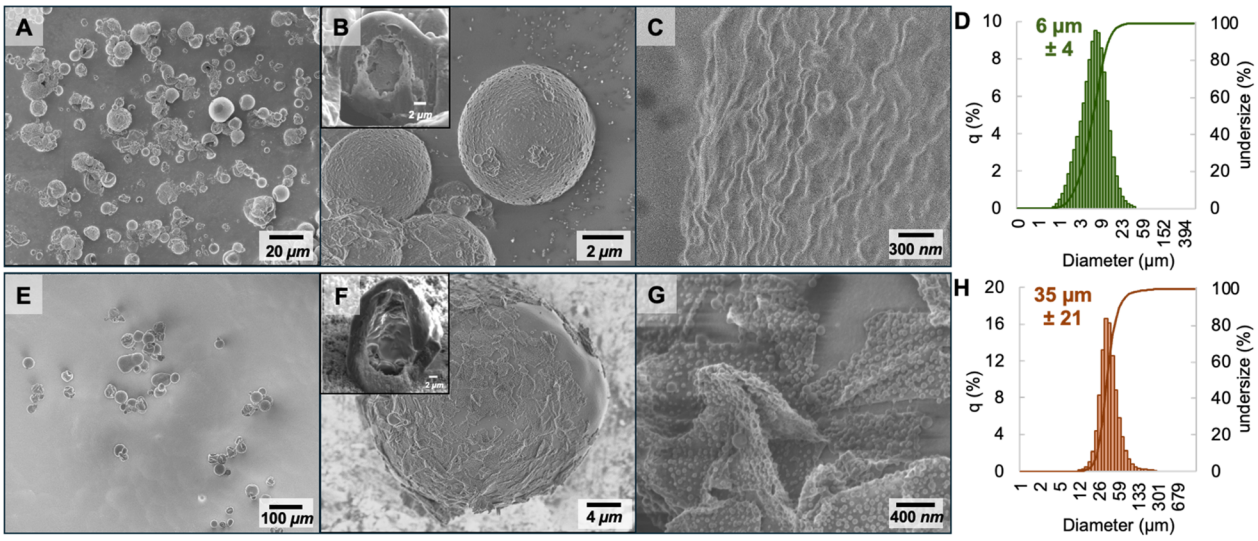

Fig. 1 SEM images and particle size analysis of (A–D) PDMS-PU capsules; and (E–H) GO-PDMS capsules. Inset in B and F are SEM-FIB images of capsule cross-sections.

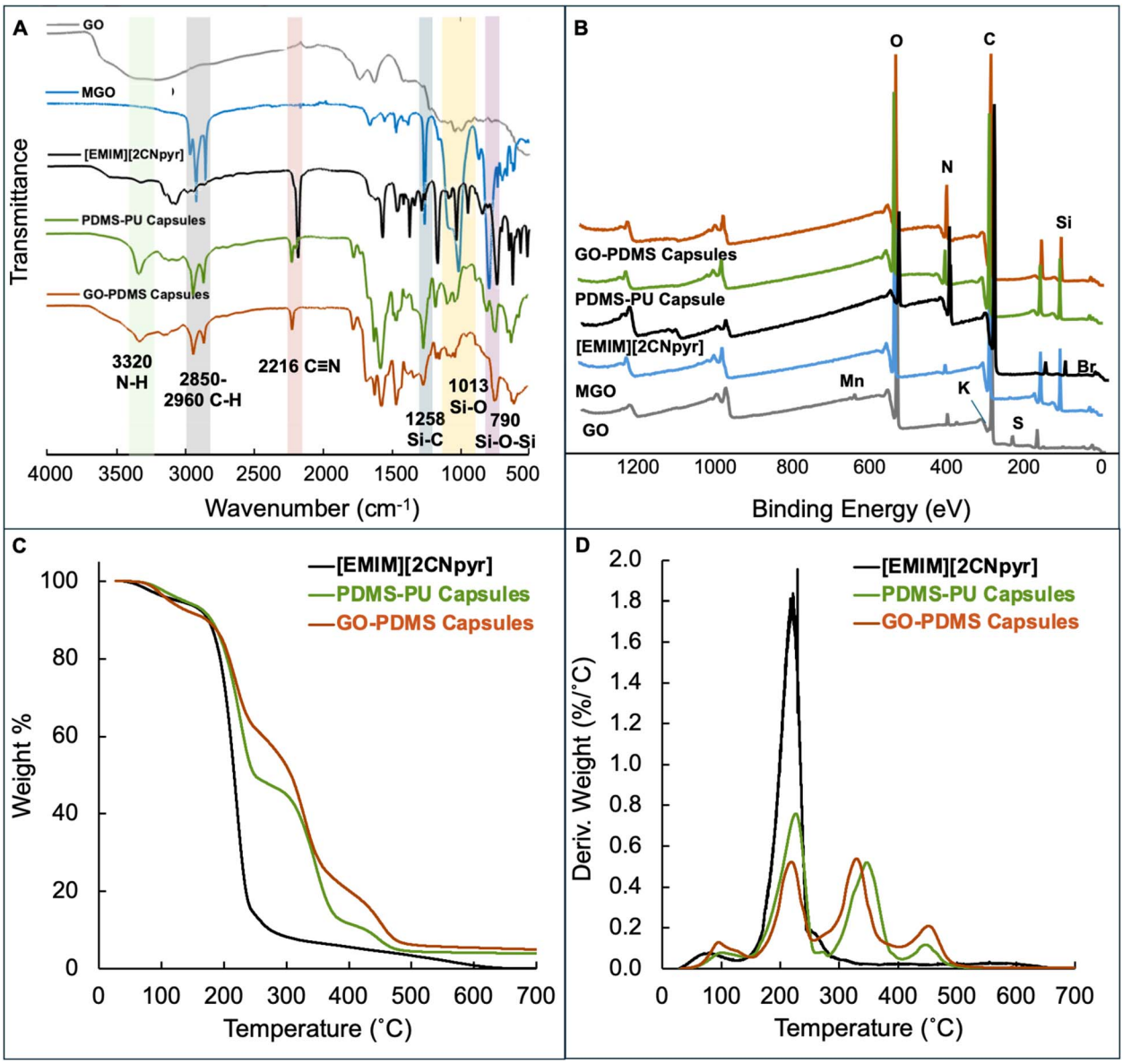

Fig. 2 (A) FTIR spectra, and (B) XPS spectra of GO-PDMS and PDMS-PU capsules, TSIL, MGO, GO. (C) TGA decomposition curves and (D) their weight loss derivative for capsules and the TSIL.

X-ray photoelectron spectroscopy (XPS) was also used to characterize the capsules and components (Fig. 2B). The XPS spectrum of the PDMS-PU capsules shows a Si 2p binding energy at ~101.8 eV, which is present in all samples but shifts slightly to higher binding energy in the capsules (Fig. S4A). Further, the primary O (19.5 at%) in the O 1s spectrum is likely O–Si bonds. The total Si surface atomic composition was 15.6 at%, confirming the presence of PDMS in the shell. The N (7.8 at%) 1s binding energy (~399 eV) is pronounced in the PDMS-PU system, indicating the presence of amines within the shell, which likely enhances CO_2 selectivity and transport. Interestingly, the N 1s spectrum of PDMS-PU capsules also shows a peak at ~401.7 eV, revealing the presence of pyrrole species from the TSIL (Fig. S4B), which suggests its incorporation in the shell. For the GO-PDMS capsules, the presence of Si–O and Si–C (~100.2–100.4 eV), which are absent in pristine GO (Fig. S4A), confirms the successful grafting of PDMS onto the nanosheets, with a total Si and O surface composition of 10.7 at% and 17.4 at%, respectively. Slightly lower than those of PDMS-PU capsules. The N 1s binding peak at ~399 eV is also present in the GO-PDMS capsules, with a slightly higher N atomic composition (N 11.0 at%) compared to PDMS-PU. Similar to PDMS-PU, a small peak at ~401.7 eV is present, also indicating the incorporation of the TSIL in the shell. The GO-PDMS capsules spectra also shows intensity at ~289 eV which is typically assigned to a carbonate, likely formed due to CO_2 binding on the surface. Table S1 summarizes the atomic percent surface composition calculated from the XPS spectra.

The thermal stability and degradation profiles of the capsules and TSIL were evaluated by thermogravimetric

analysis (TGA) under air from ambient to 700 °C. Fig. 2C shows the weight loss profiles, and Fig. 2D represents the first derivatives of those profiles. The TSIL and capsules show an initial mass loss occurring at ~80 °C, attributed to the release of absorbed solvent, moisture, and/or CO_2 from the system. The second weight loss event is observed for the TSIL at ~216 °C which is a slightly lower temperature than the second weight loss event of the capsules, which occurs at 237 °C and 227 °C for PDMS-PU and GO-PDMS, respectively, indicating a higher thermal stability of the capsules compared to the bulk TSIL, as previously reported in similar work.[29] In comparison, the capsules decompose in a similar temperature range as each other, with the PDMS-PU capsules demonstrating a slightly better thermal stability, with the second decomposition peak at 340 °C, compared to 335 °C for GO-PDMS. At CO_2 desorption temperatures (~65 °C), no significant degradation is detected, suggesting that the capsules can withstand these temperatures without significant degradation.

The liquid content of the capsules was determined by extraction and characterization using ^{1}H NMR spectroscopy. A known mass of capsules was treated with a solution of DMSO-d_6 containing mesitylene as an internal standard, then the TSIL content was quantified by integrating the mesitylene peak relative to that of the TSIL (Fig. S5). For the PDMS-PU capsules, the ^{1}H NMR spectrum of the extracted liquid (Fig. S5B) matched that of the TSIL, confirming successful encapsulation while preserving its purity. The quantification of the liquid content revealed that the capsules contained 51 wt% TSIL, which aligns with our previous core loading obtained with soft-template encapsulation.[29,41,42] Similarly, the NMR spectrum of the extracted liquid from GO-PDMS capsules showed peaks attributed to the TSIL (Fig. S5C); although the calculated loading was 20 wt% based on ^{1}H NMR analysis, gravimetric measurements based on weighing the shell before and after core extraction by grinding the capsules, indicated a loading of 53 wt% (see Table S2). This discrepancy suggests that TSIL could not readily diffuse out of the shell, which is further supported by the water immersion test discussed later, leading to an underestimation of the TSIL content by NMR alone.

CO_2 sorption performance & microwave regeneration

Fig. 3A illustrates the different CO_2 reaction mechanisms with [EMIM][2CNpyr], as previously reported.[40,62–64] Under dry conditions, CO_2 can react with the anion to form carbamate (route 1) or with a transient carbene derived from the deprotonated cation to produce imidazolium carboxylate (route 2). In the presence of moisture, CO_2 primarily reacts with hydroxide produced by reaction of water and the anion, leading to bicarbonate formation (route 3). The same reaction mechanisms are expected to occur in the encapsulated TSIL as for the bulk.

The gravimetric CO_2 uptake performance for both types of capsules was evaluated at 30 °C under pure CO_2 and DAC conditions (410 ppm CO_2 in N_2), comparing to the TSIL itself.

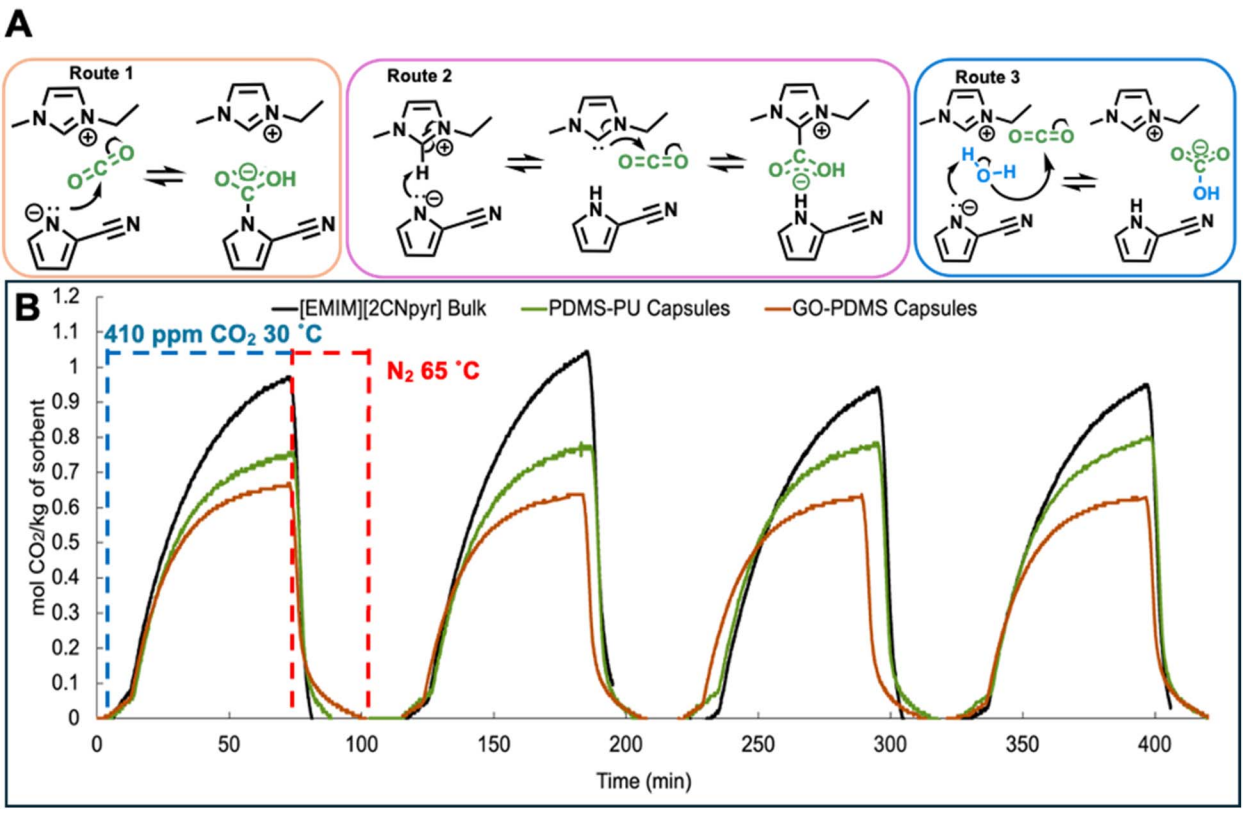

Fig. 3 (A) Reaction pathways of the TSIL [EMIM][2CNpyr] with CO_2 following 3 different routes.[40] (B) Capsules CO_2 sorption and thermal regeneration over four cycles: measured gravimetrically at 1 bar of 410 ppm CO_2 at 30 °C for sorption, then desorption at 65 °C under 1 bar N_2.

Each sample was first pretreated by heating at 65 °C under 1 bar of N_2 for 1 hour to remove volatiles and adsorbed water or CO_2 from air; these conditions were chosen to reflect thermal regeneration conditions. To assess the contribution of the shell materials to CO_2 uptake, hollow shells were prepared by extracting the core liquid (see SI for details); DAC capacities of 0.04 and 0.03 mol kg^{-1} were observed for PDMS-PU and GO-PDMS, respectively (Fig. S6A). At 1 bar of pure CO_2, the TSIL (*i.e.*, pure [EMIM][2CNpyr]) reached a plateau in mass gain reflecting a capacity of 5 mol kg^{-1}, as previously reported.[40] For the PDMS-PU capsules, CO_2 sorption at 1 bar of pure CO_2 resulted in a capacity of 2.4 mol kg^{-1} (Fig. S6B). The capsules reached the equilibrium capacity faster than the bulk TSIL, likely due to enhanced transport properties for the encapsulated system (*e.g.*, higher accessible surface area). Further, after normalizing the TSIL capacity (5 mol kg^{-1}) to the core content (51 wt%), the capsules' capacity aligns with expectations (2.55 mol kg^{-1}), confirming that the capsules reach pseudo-equilibrium capacity. The pure CO_2 gravimetric capacity of the GO-PDMS capsules was measured at 3.2 mol kg^{-1}. Unlike PDMS-PU, the observed uptake capacity is slightly higher than the expected TSIL capacity of ~2.65 mol kg^{-1}, suggesting that the wt% loading of these capsules is potentially slightly higher than that calculated gravimetrically due to plasticized TSIL. These results suggest that the shell accommodates CO_2 diffusion by facilitated transport from the shell to the inner liquid core.

The DAC gravimetric capacities of the capsules and cyclability compared to the TSIL bulk liquid is shown in Fig. 3B, where the sorption was performed under 410 ppm CO_2 in N_2 (1 bar) and 30 °C, and desorption performed under N_2 (1 bar) and 65 °C. The TSIL had a capacity of 0.97 mol kg^{-1} in the first cycle, slightly higher than that previously reported (0.75 mol kg^{-1});[10] this may be due to the difference in measurement techniques, as our approach gravimetrically measures the pseudo-equilibrium with TGA and the previously reported capacity utilizes ^{13}C NMR spectroscopy and integration of specific, broad peaks. Under the TGA conditions, the DAC performance of the TSIL is relatively stable upon cycling using thermal regeneration. For the PDMS-PU capsules, the measured capacity was 0.76 mol kg^{-1} in the first cycle, and slightly increased to 0.80 mol kg^{-1} by the 4th cycle. Based on the 51 wt% TSIL content and the capacity of the TSIL bulk, the expected capacity of the PDMS-PU capsules was 0.49 mol kg^{-1}; however, the capsules exceeded this value by 55%, suggesting CO_2 uptake beyond the predicted equilibrium capacity due to the increased surface area, leading to better availability of CO_2 reactive sites and overcoming mass transport limitations. Similarly, the GO-PDMS capsules reached a capacity of 0.66 mol kg^{-1} during the first exposure to DAC conditions and showed a stable capacity over the next three cycles, with a 35% increase in capacity compared to the expected value (0.49 mol kg^{-1}). Both PDMS-PU and GO-PDMS capsules exhibit similar rates of uptake and comparable capacities, indicating that the incorporation of GO does not significantly compromise mass transport of CO_2 through the shell and the inherent chemisorptive preference of the TSIL. These results confirm that the encapsulation of the TSIL leads to increased accessible surface area which mitigates mass transport of CO_2 found in bulk liquid limitations. Further, the CO_2 over N_2 selectivity is also potentially enhanced by introducing GO nanosheets into the shell composition, which create narrower channels that only allow the small CO_2 molecules to diffuse through, and blocking the larger N_2 molecules. The stability of both capsule types was tested over 12 cycles of DAC sorption (410 ppm CO_2 30 °C) and desorption (N_2 at 65 °C) as an initial screening to assess reversible uptake and regeneration behavior, and to determine their stability and capacity retention (Fig. S6C). While there was a slight reduction in capacity for PDMS-PU, both capsule types demonstrated good stability. Specifically, after 12 cycles, the PDMS-PU and GO-PDMS capsules retained 76% and 82% of their DAC capacity, respectively.

Breakthrough DAC performance of the capsules was evaluated using the setup shown in the inset of Fig. 4A. An ideal breakthrough curve for a DAC material is typically characterized by three criteria: an initial flat baseline indicating that the sorbent is effectively capturing all incoming CO_2, followed by a steep rise in CO_2 concentration indicating the material is approaching saturation, and finally a quick leveling as the effluent reaches the concentration of the inlet CO_2, reflecting the saturation of the material. The breakthrough curves of both capsule types were obtained to evaluate their kinetics and working capacities. Briefly, around 300 mg of the capsules were packed into a PTFE column then heated under reduced pressure at 65 °C overnight to remove absorbed CO_2 prior to the breakthrough experiments, then the system was allowed to cool to 25 °C while purging with pure Ar. The flow rate of the experiment was set to 0.18 L min^{-1}, maintained by mass flow controllers.

To the pretreated column of capsules, the gas feed was switched to 410 ppm CO_2 and a breakthrough curve was obtained for both types of capsules (Fig. 4A). The PDMS-PU capsules exhibited a shorter breakthrough time (5% of the feed concentration) than the GO-PDMS capsules, suggesting that CO_2 diffusion is slower in PDMS-PU as the breakthrough time is the point at which the column is no longer absorbing CO_2 as fast as CO_2 is being fed. The pseudoequilibrium time, the point at which the CO_2 concentration in the effluent stabilizes and the capsules are near full saturation (>95% of the feed concentration), was nearly twice as long for PDMS-PU compared to GO-PDMS, suggesting that PDMS-PU is diffusion limited; however, this contradicts the results obtained with the TGA sorption under 420 ppm CO_2 (Fig. 3B), where the PDMS-PU capsules showed similar sorption rates as the GO-PDMS. Further, under gravimetric pure CO_2 uptake, PDMS-PU showed higher sorption rates than GO-PDMS (Fig. S6B). This suggests that while PDMS-PU shell is permeable (further supported by the water immersion results discussed below and in Fig. S8), its CO_2 selectivity may be reduced due to CO_2-induced plasticization of the polymer shell; an effect well documented for gas separation membranes,[65–69] which leads to slow breakthrough kinetics.[70]

In contrast to PDMS-PU, the GO-PDMS capsules exhibited a significantly longer breakthrough time, indicating that

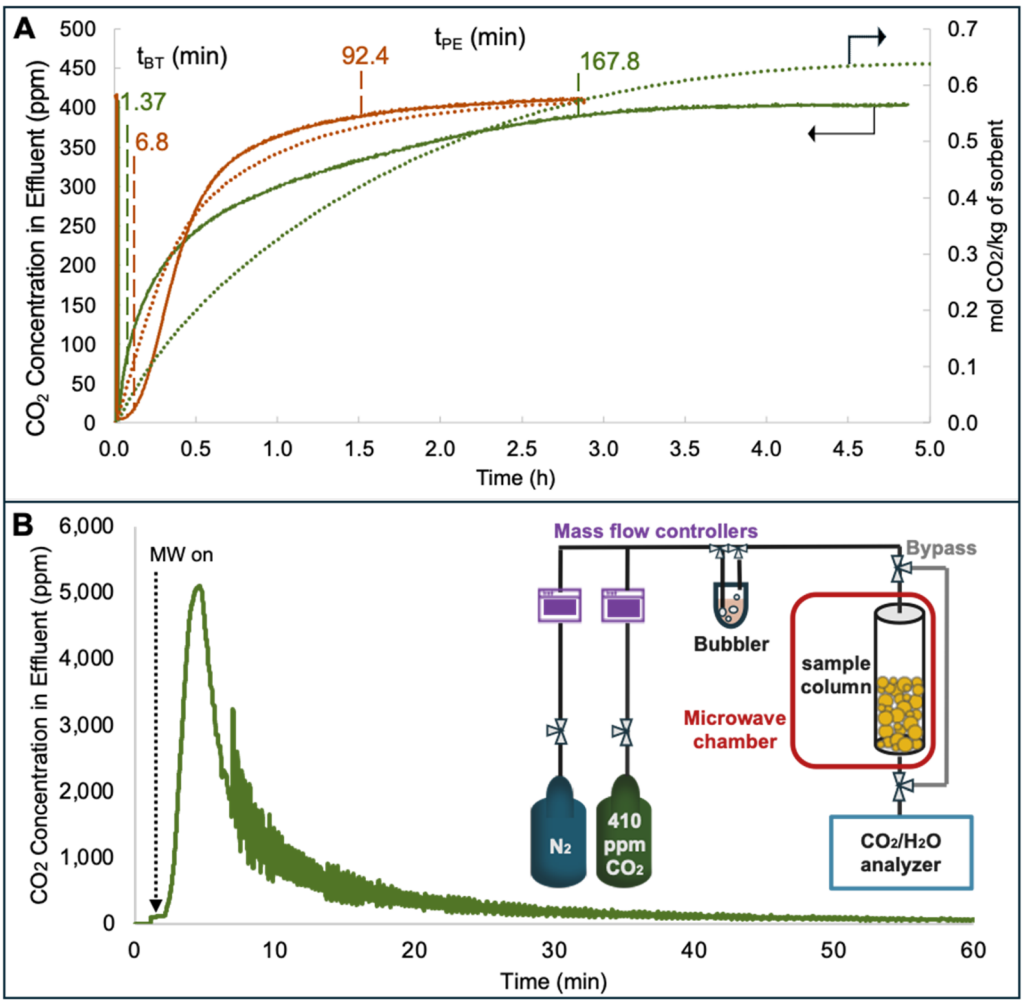

Fig. 4 (A) Breakthrough curves of PDMS-PU (green) and GO-PDMS (orange) capsules with inset showing schematic of breakthrough apparatus, 410 ppm CO_2. (B) Microwave regeneration (65 °C) of PDMS-PU at 5 W.

absorption in this column was able to keep up with the rate of CO_2 being fed for longer. The breakthrough curve also shows a steeper rise in CO_2 concentration in the effluent compared to the PDMS-PU capsules. This runs counter to expectations based on the size distribution of the capsules, as the smaller PDMS-PU capsules are expected to saturate more quickly due to the shorter diffusion distance. However, incorporating GO into the shell increases the shell's selectivity by introducing a layered, size-sieving architecture that limits molecular diffusion through the polymer. The GO nanosheets create tortuous diffusion pathways within the PDMS matrix, effectively acting as a physical barrier to larger molecules while allowing the smaller CO_2 molecules to permeate efficiently. This increased permeation selectivity explains why the kinetics of the GO-PDMS capsules are better than that of the PDMS-PU capsules, despite the larger size of the GO-PDMS capsules.[71–73] Further, the packing of the column can also significantly influence measured breakthrough kinetics: a tightly packed column increases pressure drop and prolongs gas-sorbent contact, delaying breakthrough, whereas a loosely packed column may contain voids or channels that allow gas to bypass the sorbent, leading to early breakthrough. In this study, the substantial size difference and distinct shell properties between the two capsule types could affect their packing density, affecting gas flow patterns and contact efficiency, and thereby contributing to the observed differences in breakthrough behavior. And yet, both capsules exhibited similar CO_2 breakthrough capacities of 0.64 and 0.57 mol kg^{-1} for PDMS-PU and GO-PDMS, respectively, which are slightly lower values that those obtained from gravimetric studies described above (Table 1), as expected for this methodology.

Microwave and radio frequency regeneration

Key aspects of lowering the operational cost of DAC include not only maintaining the performance over numerous cycles, but also lowering the energy required for regeneration. One way to reduce energy consumption is by using electrothermal heating, as opposed to convection heating, in two different regimes: microwave (MW) and radio frequency (RF). When exposed to MW, the TSIL heats up rapidly due to its dipolar nature, where the ions interact with the electromagnetic field, leading to faster

Table 1 Breakthrough results for the synthesized capsules

	t_{BT} (min)	t_{PE} (min)	PE CO_2 capacity (mol kg^{-1})	Saturation capacity from breakthrough (mol kg^{-1})	TGA capacity (mol kg^{-1})
PDMS-PU	1.4	167.8	0.57	0.64	0.75
GO-PDMS	6.8	92.4	0.53	0.57	0.66

and more uniform heating compared to conventional methods. Following CO_2 uptake using the breakthrough set up, MW was applied to the PDMS-PU capsules (Fig. 4A inset). The gas was switched to nitrogen at 0.2 L min^{-1} flow rate and the CO_2 concentration in the effluent was measured as a function of time as MW was applied at 5 W to heat the sample to 65 °C, as determined by an IR temperature sensor (Fig. 4B). A rapid initial desorption of CO_2 was observed in the first 10 min, evident by a dramatic increase in CO_2 concentration in the effluent, reaching 5000 ppm in the first 5 minutes. After the initial spike in desorption, slower CO_2 loss from the capsules was observed, which we attribute to CO_2 moving from the liquid core to the shell, then leaving the capsule. Complete regeneration was observed in less than an hour, as evidenced by the CO_2 concentration in the effluent being 0 ppm. While MW regeneration has proven promising for DAC materials,[10,52,53] as demonstrated in our *in situ* sorption and desorption, applying MW at scale may be challenging that could create hot-spots in a fixed, packed column of solid sorbent-ideally a fluidized bed would allow for thermal equilibration of materials as one potential solution. Further, while the PDMS-PU capsules were regenerated using MW heating, the GO-PDMS capsules were instead regenerated with RF heating. This choice was motivated by the conductive nature of GO. Given the MW instrument's minimum output of 5 W, using it to heat the GO-PDMS can risk thermal degradation of the capsules.

An alternative low energy heating approach is to utilize RF, which interacts strongly with polar molecules and conductive materials, such as the nanosheets in the GO-PDMS capsules. RF heating generates a more uniform electromagnetic field and uses lower frequencies than MW, more importantly, our RF setup allows for modulation of lower power output than the MW (as low as 1 W), a key feature that enables controlled and gradual heating of conductive materials like GO-PDMS capsules. This significantly reduces the risk of hot spots and material degradation that would otherwise occur at higher power levels. Indeed, RF has been previously shown to heat GO-containing structures.[58] Using the setup shown in Fig. 5A, the capsule samples were placed on a fringing field applicator, and exposed to an RF field generated using a signal generator. The amplified signal was then directed to the applicator, where a thermal camera was used to monitor the temperature of the sample. Prior to heating the capsules, a Vector Network Analyzer (VNA) was used on the neat (CO_2 free) sample to determine the best radio frequencies the capsules interact with and show heating (Fig. 5B). The sample showed a strong absorption (lowest S_{11} values) at 129 and 143 MHz.

To determine the frequency at which the capsules heated best, the rate of heating as a function of frequency was

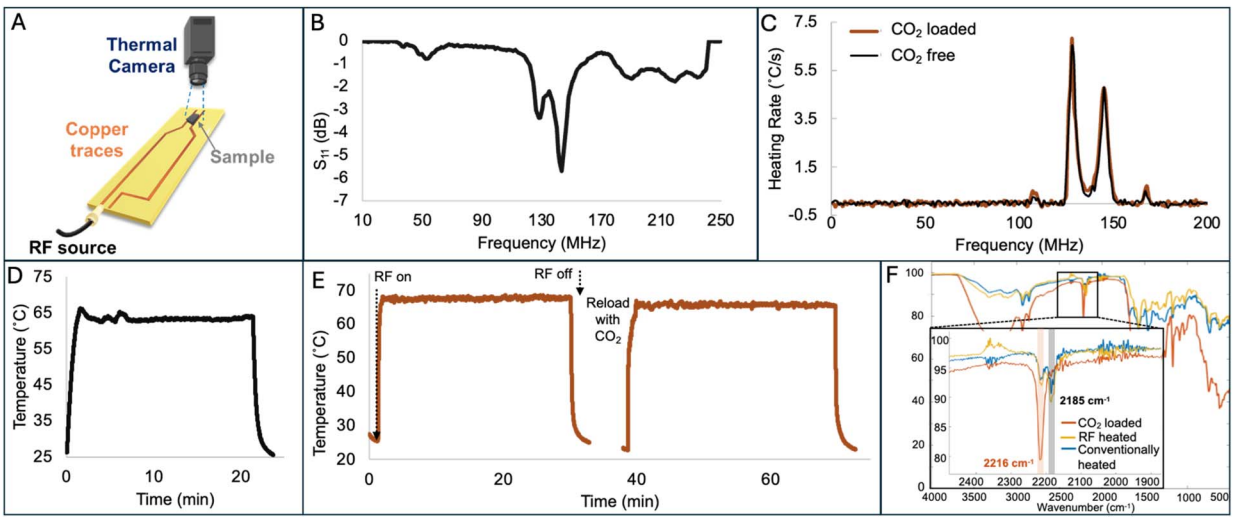

Fig. 5 (A) RF setup demonstrating placement of sample and thermal camera, (B) VNA graph of applicator and GO-PDMS capsules without CO_2, (C) Frequency sweep (0–200 MHz, 2 W) of GO-PDMS capsules before and after CO_2 loading, performed by turning RF on for 1 s to heat the sample and off for 13 s to cool the sample at each frequency step. (D) Heating of lean GO-PDMS capsules (without CO_2) at 1–2 W and 140 MHz, (E) Regeneration of CO_2 loaded GO-PDMS capsules at 1–2 W and 128 MHz. (F) FTIR spectra of GO-PDMS capsules before and after RF heating. Black lines represent CO_2-lean capsules and orange lines represent CO_2-loaded capsules.

measured: RF was turned on at 2 W for 1 second then turned off for 13 seconds (Fig. 5C) and the frequency was then increased in 1 MHz steps. This frequency sweep was carried out from 1 MHz to 200 MHz. The heating rate at each frequency was calculated by analyzing the slope of the initial linear region in the temperature–time plot. The GO-PDMS capsules show the highest heating rate at 128 MHz, and second highest rate at 145 MHz. Two additional small peaks are observed at 109 and 168 MHz. Both lean and CO_2 loaded samples show the similar heating frequencies. It is noteworthy to mention that these frequencies can vary slightly due to minor changes in the setup and location of the sample on the applicator. The RF heating of GO-PDMS capsules was first tested on the as prepared sample, where RF was applied at 140 MHz and the power was modulated between 1–2 W to effectively maintain temperature of the sample at 65 °C. As shown in Fig. 5D, the capsules reached 65 °C within seconds and remained at a constant temperature for 20 min. RF was then applied to capsules that had been loaded with CO_2 (128 MHz and 1–2 W to maintain ~65 °C for 30 min, Fig. 5E); this was the same temperature and time that led to full regeneration of the capsules in the TGA experiments as described above. Two cycles of heating were performed, where CO_2 was reintroduced into the capsules after the first regeneration to demonstrate cycling performance. CO_2-loaded and CO_2-lean capsules demonstrate similar patterns of instant heating in response to RF to reach the targeted temperature, and the samples stayed at that temperature for the given timeframe. Notably, the frequency needed to heat the capsules was consistent regardless of if CO_2 was loaded, which supports the opportunity to standardize a method for RF regeneration.

To confirm that CO_2 was effectively desorbed, FTIR spectra of the CO_2-loaded, conventionally-heated, and RF-heated capsules were collected (Fig. 5F). As discussed above, the stretching frequency of the cyano group shifted from 2185 cm^{-1} for pristine TSIL to 2216 cm^{-1} upon CO_2 binding. Such shift is observable, even after loading the capsules under DAC conditions.[61] The FTIR spectra of both heated samples have both peaks, but the CO_2 loaded sample shows only 1 peak at 2216 cm^{-1} (Fig. 5F), suggesting that both RF heated and conventionally heated samples adequately desorbed CO_2 but ambient atmosphere (*i.e.*, DAC CO_2 concentration) leads to rapid carbon capture. RF heating was also applied to the PDMS-PU capsules, with heating expected due to the ionic conductivity of the TSIL, as previously reported;[74] here, regeneration temperature (65 °C) was reached within seconds at 1–2 W, and the temperature was maintained for 20 minutes (Fig. S7).

Water stability

Another important factor to consider in developing DAC materials is stability to water, because any uptake of water could lead to the formation of carbonate salts which require a significantly higher temperature for regeneration (*e.g.*, 90 °C).[10] For the GO-PDMS capsules, in addition to providing controlled absorption kinetics and conductivity for RF heating, we discovered that the hydrophobicity of MGO provided superior water stability. Fig. 6 shows the TGA sorption profile of the GO-PDMS capsules after they were submerged in DI water for 24 hours, then filtered and dried under reduced pressure. The capacities before and after submersion in water show a slight difference, with the water-

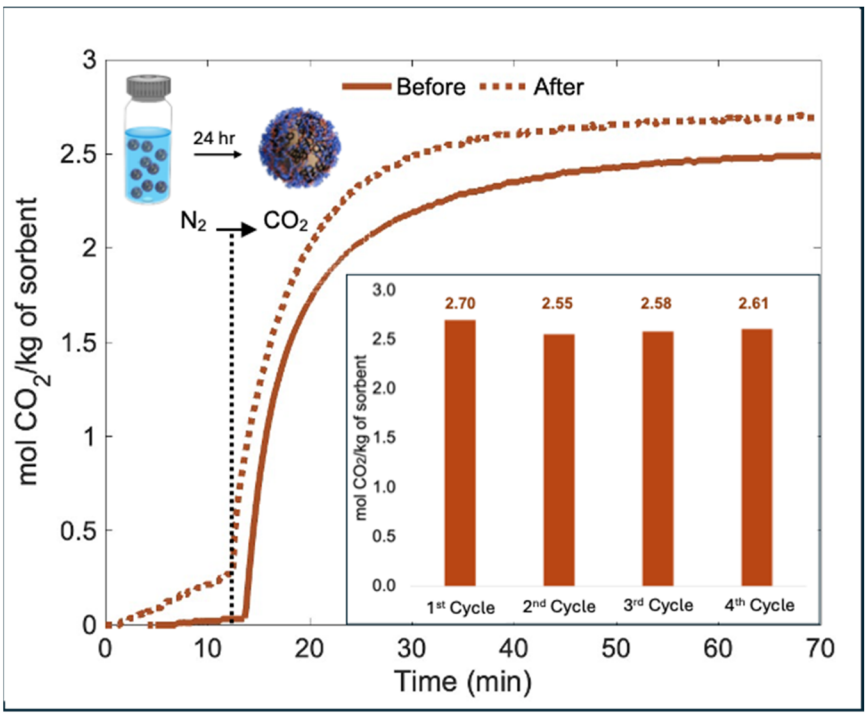

Fig. 6 Gravimetric CO_2 capacities of the GO-PDMS capsules (1st cycle) before and after submersion in water. Inset shows CO_2 sorption cycles of the water-submerged sample regenerated at 65 °C under N_2. Sorption conditions: 1 bar CO_2, 30 °C.

Table 2 DAC-relevant CO_2 capacities under dry conditions of similar core–shell IL/TSIL composites reported in the literature in comparison to this work

Solid–liquid composite	Liquid wt%	Temp. (°C)	Pressure (bar)	CO_2 partial pressure (mbar)	CO_2 capacity (mol kg^{-1})	Cycles, capacity lost	Ref.
[EMIM][2CNpyr] PDMS-PU	51	30	1	0.41	0.76	12, 24%	This study
[EMIM][2CNpyr] GO-PDMS	53				0.66	12, 24% loss	
[EMIM][2CNpyr]@PU	25	25	1	0.5	0.16		41
[EMIM][2-CNpyr]/1,3-P@PU	28				0.47	9, 15%[a,b]	
[EMIM][2CNpyr]/DEG@PU	34				0.66	9, 19%[a,b]	
[EMIM][2CNpyr]@PU	60	25	—	5	0.82	2, —	40
[EMIM][2-CNpyr]/ZIF-8	35	30	1	0.5	0.20	10, 15%	52
			0.001	1	0.16	—	
			0.005	5	0.40	—	
			1	1000	1.28	—	
[BMIM][BF_4]/MEA GO-PU	64	25	1	0.5	0.02	—	29
[BMIM][BF_4]/MEA/Pz GO-PU	51				0.04	10, 14%[a]	
[MeTBDH]2[HFPDO]/Ni-MOF	1.74[c]c	25	—	0.4	0.58	5, 4.6%	75
Zeolite 13X[d]	—	25	0.0005	0.5	0.4	100, 27%[a]	76 and 77
			1	1	1.2	—	76
				3	2.1	—	

[a] Cycling performed under 1 bar CO_2. [b] Loss observed only after the first cycle. [c] SIL mmol g^{-1} MOF. [d] Not a solid–liquid composite.

submerged sample having a slightly higher capacity (30 °C, 1 bar CO_2). This may be due to diffusion of water into the capsules which promotes formation carbonates and bicarbonates; however, the performance also suggests that the TSIL is not extracted from the capsules. For the capsules which had been submerged in water, the capacity was measured over 4 cycles, showing negligeable changes (Fig. 6 inset). The same test was performed for the PDMS-PU capsules, revealing a drastic decrease in capacity for the sample after submersion in water (2.4 to 0.2 mol kg^{-1} for as-prepared and water-submerged samples, respectively); this can be attributed to the TSIL being extracted into the water (Fig. S8).

To highlight the modularity of our emulsion-templated method, different CO_2-absorbing liquids were encapsulated. Fig. S9 shows optical microscopy images of capsules with both types of shells (PDMS-PU and GO-PDMS) containing a core of the IL [BMIM][BF_4] (Fig. S9A and C) or polyethyleneimine (PEI), a polyamine known to chemisorb CO_2 (Fig. S9B and D). This demonstrates the versatility of the method and the ability to accommodate a wide variety of CO_2-absorbing liquids, expanding their potential compositions and application spaces. Further, among similar composites, these materials have shown significant enhancement in performance, summarized in Table 2.

Conclusion

We successfully designed and synthesized PDMS-based microcapsules for DAC application and electrothermal heating regeneration. The favorable performance of the capsules under DAC can be attributed to high shell permeability to CO_2, achieved by incorporating a flexible PDMS polymer, and liquid core of the TSIL [EMIM][2CNpyr]. Two types of PDMS-composite capsules were fabricated *via* emulsion templating, using PDMS as a surfactant and growing polyurea at the interface of the droplets or using MGO sheets as a surfactant and cross-linking them with PDMS. Additionally, electrothermal heating; microwave (MW) and radio frequency (RF), were investigated as alternative regeneration approaches to improve efficiency and reduce operational costs. The two systems exhibited performance differences, attributed to differences in shell structure and composition. The PDMS-PU capsules demonstrated CO_2 capacities up to 0.8 mol kg^{-1} at 410 ppm CO_2, outperforming previous liquid-filled capsules investigated for DAC. These capsules exhibited compatibility with both MW and RF regeneration methods, where MW regeneration was rapid and energy-efficient (5 W, full desorption in <30 min at 65 °C), similar to RF heating (2 W, stable heating >30 min at 65 °C). However, under realistic setup they have slower kinetics due to low CO_2 over N_2 selectivity, and are not water stable, which limits performance under humid conditions. As for the GO-PDMS capsules, while slightly lower CO_2 DAC capacities (0.66 mol kg^{-1}) were observed compared to PDMS-PU, these capsules showed a more favorable mass transfer behavior due to their size-sieving properties. The GO-PDMS capsules were also compatible with RF regeneration, requiring very low energy to maintain 65 °C (<2 W). More importantly, however, is the hydrophobic nature and structural robustness of the shell, giving these capsules superior water stability, making them more ideal for realistic humid uptake conditions. In conclusion, both capsule types demonstrated reasonable DAC capacities, kinetics, and cyclability under dry conditions; however, the choice between the two depends on the operational priorities: maximizing uptake and utilizing MW for regeneration *vs.* tuning permeability and utilizing RF-heating regeneration.

Our current studies focus on optimization needed to address efficient large-scale implementation. While the capsules demonstrate potential in DAC application with low energy requirements, further research is needed to elucidate the CO_2

diffusion mechanism through the shell, assessing the effects of humidity and acidic environments, and evaluating long-term stability and cyclability. Additionally, batch to batch variations were observed due to the multi-step synthetic procedure. Both capsules require simplification in formulation methods to ensure a consistent scale-up and utilizing cost-effective and commercially available materials. Further, electrothermal heating (both MW and RF) is being studied under realistic conditions, such as humidity effects. Lastly, safety concerns and precautions need to be addressed with the scale-up of these regeneration approaches.

Conflicts of interest

The authors declare no conflict of interest.

Data availability

The data that support the findings of this study are available in the supplementary information (SI) of this article. Supplementary information: OM images of the capsules, MGO FTIR spectra, XPS spectra, ^{1}H NMR spectra and wt% calculations, gravimetric CO_2 sorption curves of capsules, hollow shells, and cycling performance, RF heating of PDMS-PU capsules, DAC gravimetric performance of PDMS-PU after water immersion, OM images of other encapsulated core liquids. See DOI: https://doi.org/10.1039/d5ta08055j.

Notice

Acknowledgements

L. A. synthesized the capsules and conducted characterizations. Y. Y. obtained SEM images. H. M. M. conducted XPS experiments. L. A. and S. D. conducted RF heating experiments supervised by M. J. G. A. K. conducted breakthrough and MW heating experiments. L. A. prepared the original draft, and all authors reviewed and edited the manuscript. M. K. K. and E. P. conceptualized, supervised and acquired funding for this research. We are grateful for the contributions of Yi-Feng Su who obtained SEM-FIB images Oak Ridge National Laboratory. The use of the Texas A&M University Soft Matter Facility (RRID: SCR 022482), and the Texas A&M University Materials Characterization Core Facility (RRID: SCR_022202) are acknowledged. SEM was conducted as part of a user project at the Center for Nanophase Materials Sciences (CNMS), which is a U. S. Department of Energy, Office of Science User Facility at Oak Ridge National Laboratory. This material is based upon work supported by the U. S. Department of Energy (Award No. DE-SC0022214), L. A. participated in the DOE-GRO program in which allowed access to ORNL to carry out this research.

References

1 U.S. Department of Energy, The Role of Carbon Capture, Utilization, and Storage in Forming a Low-Carbon Economy. https://www.energy.gov/articles/role-carbon-capture-utilization-and-storage-forming-low-carbon-economy, accessed 2025-05-19.
2 U.S. Department of Energy, DOE Awards $20 Million to Help States Deploy Carbon Capture and Storage, https://www.energy.gov/articles/doe-awards-20-million-help-states-deploy-carbon-capture-and-storage, accessed 2025-05-30.
3 J. Valentine, A. Zoelle, S. Homsy, H. Mantripragada, A. Kilstofte, M. Sturdivan, M. Steutermann and T. Fout, *Direct Air Capture Case Studies: Solvent System, DOE/NETL-2021/2864*, 2022, p. 1893369, DOI: 10.2172/1893369.
4 M. Erans, E. S. Sanz-Pérez, D. P. Hanak, Z. Clulow, D. M. Reiner and G. A. Mutch, Direct Air Capture: Process Technology, Techno-Economic and Socio-Political Challenges, *Energy Environ. Sci.*, 2022, **15**(4), 1360–1405, DOI: 10.1039/D1EE03523A.
5 M. Ozkan, S. P. Nayak, A. D. Ruiz and W. Jiang, Current Status and Pillars of Direct Air Capture Technologies, *iScience*, 2022, **25**(4), 103990, DOI: 10.1016/j.isci.2022.103990.
6 R. R. Bottoms, *Process for Separating Acidic Gases*, 1930.
7 Y. Jin, H. Lin, Y. Liu, H. An and J. S. Lee, Optimizing Amine-Based Adsorbents for Direct Air Capture: A Comprehensive Review of Performance under Diverse Climatic Conditions, *Renew. Sustain. Energy Rev.*, 2025, **217**, 115782, DOI: 10.1016/j.rser.2025.115782.
8 E. Medina-Martos, J.-L. Gálvez-Martos, J. Almarza, C. Lirio, D. Iribarren, A. Valente and J. Dufour, Environmental and Economic Performance of Carbon Capture with Sodium Hydroxide, *J. CO2 Util.*, 2022, **60**, 101991, DOI: 10.1016/j.jcou.2022.101991.
9 E. A. Recker, M. Green, M. Soltani, D. H. Paull, G. J. McManus, J. H. Davis and A. Mirjafari, Direct Air Capture of CO_2 *via* Ionic Liquids Derived from "Waste" Amino Acids, *ACS Sustain. Chem. Eng.*, 2022, **10**(36), 11885–11890, DOI: 10.1021/acssuschemeng.2c02883.
10 Y. Lee, E. Cagli, A. Klemm, Y. Park, R. Dikki, M. K. Kidder and B. Gurkan, Microwave Regeneration and Thermal and Oxidative Stability of Imidazolium Cyanopyrrolide Ionic Liquid for Direct Air Capture of Carbon Dioxide, *ChemSusChem*, 2023, **16**(13), e202300118, DOI: 10.1002/cssc.202300118.
11 P. Husson-Borg, V. Majer and M. F. Costa Gomes, Solubilities of Oxygen and Carbon Dioxide in Butyl Methyl Imidazolium Tetrafluoroborate as a Function of Temperature and at Pressures Close to Atmospheric

Pressure, *J. Chem. Eng. Data*, 2003, **48**(3), 480–485, DOI: 10.1021/je0256277.

12 C. Cadena, J. L. Anthony, J. K. Shah, T. I. Morrow, J. F. Brennecke and E. J. Maginn, Why Is CO_2 So Soluble in Imidazolium-Based Ionic Liquids?, *J. Am. Chem. Soc.*, 2004, **126**(16), 5300–5308, DOI: 10.1021/ja039615x.

13 M. B. Shiflett and A. Yokozeki, Solubilities and Diffusivities of Carbon Dioxide in Ionic Liquids: [Bmim][PF_6] and [Bmim][BF_4], *Ind. Eng. Chem. Res.*, 2005, **44**(12), 4453–4464, DOI: 10.1021/ie058003d.

14 A. N. Soriano, B. T. Doma and M.-H. Li, Carbon Dioxide Solubility in 1-Ethyl-3-Methylimidazolium Trifluoromethanesulfonate, *J. Chem. Thermodyn.*, 2009, **41**(4), 525–529, DOI: 10.1016/j.jct.2008.11.001.

15 B. E. Gurkan, J. C. De La Fuente, E. M. Mindrup, L. E. Ficke, B. F. Goodrich, E. A. Price, W. F. Schneider and J. F. Brennecke, Equimolar CO_2 Absorption by Anion-Functionalized Ionic Liquids, *J. Am. Chem. Soc.*, 2010, **132**(7), 2116–2117, DOI: 10.1021/ja909305t.

16 A. Li, Z. Tian, T. Yan, D. Jiang and S. Dai, Anion-Functionalized Task-Specific Ionic Liquids: Molecular Origin of Change in Viscosity upon CO_2 Capture, *J. Phys. Chem. B*, 2014, **118**(51), 14880–14887, DOI: 10.1021/jp5100236.

17 G. Cui, J. Wang and S. Zhang, Active Chemisorption Sites in Functionalized Ionic Liquids for Carbon Capture, *Chem. Soc. Rev.*, 2016, **45**(15), 4307–4339, DOI: 10.1039/C5CS00462D.

18 A. N. Keller, C. L. Bentley, O. Morales-Collazo and J. F. Brennecke, Design and Characterization of Aprotic *N*-Heterocyclic Anion Ionic Liquids for Carbon Capture, *J. Chem. Eng. Data*, 2022, **67**(2), 375–384, DOI: 10.1021/acs.jced.1c00827.

19 K. E. Gutowski and E. J. Maginn, Amine-Functionalized Task-Specific Ionic Liquids: A Mechanistic Explanation for the Dramatic Increase in Viscosity upon Complexation with CO_2 from Molecular Simulation, *J. Am. Chem. Soc.*, 2008, **130**(44), 14690–14704, DOI: 10.1021/ja804654b.

20 P. Priyadarshini, G. Rim, C. Rosu, M. Song and C. W. Jones, Direct Air Capture of CO_2 Using Amine/Alumina Sorbents at Cold Temperature, *ACS Environ. Au*, 2023, **3**(5), 295–307, DOI: 10.1021/acsenvironau.3c00010.

21 A. Ahmadian Hosseini and M. Jahandar Lashaki, A Comprehensive Evaluation of Amine-Impregnated Silica Materials for Direct Air Capture of Carbon Dioxide, *Sep. Purif. Technol.*, 2023, **325**, 124580, DOI: 10.1016/j.seppur.2023.124580.

22 B. Wen, Y. Li, C. Liang, Y. Chen, Y. Zhao and Q. Wang, Recent Progress on Porous Carbons for Carbon Capture, *Langmuir*, 2024, **40**(16), 8327–8351, DOI: 10.1021/acs.langmuir.3c03876.

23 D. Panda, V. Kulkarni and S. K. Singh, Evaluation of Amine-Based Solid Adsorbents for Direct Air Capture: A Critical Review, *React. Chem. Eng.*, 2023, **8**(1), 10–40, DOI: 10.1039/D2RE00211F.

24 A. A. Al-Absi, A. M. Benneker and N. Mahinpey, Amine Sorbents for Sustainable Direct Air Capture: Long-Term Stability and Extended Aging Study, *Energy Fuels*, 2024, **38**(10), 8938–8950, DOI: 10.1021/acs.energyfuels.4c01328.

25 S. Bose, D. Sengupta, T. M. Rayder, X. Wang, K. O. Kirlikovali, A. K. Sekizkardes, T. Islamoglu and O. K. Farha, Challenges and Opportunities: Metal–Organic Frameworks for Direct Air Capture, *Adv. Funct. Mater.*, 2024, **34**(43), 2307478, DOI: 10.1002/adfm.202307478.

26 X. Zhang, H. Zhao, Q. Yang, M. Yao, Y. Wu and Y. Gu, Direct Air Capture of CO2 in Designed Metal-Organic Frameworks at Lab and Pilot Scale, *Carbon Capture Sci. Technol.*, 2023, **9**, 100145, DOI: 10.1016/j.ccst.2023.100145.

27 J. J. Vericella, S. E. Baker, J. K. Stolaroff, E. B. Duoss, J. O. Hardin, J. Lewicki, E. Glogowski, W. C. Floyd, C. A. Valdez, W. L. Smith, J. H. Satcher, W. L. Bourcier, C. M. Spadaccini, J. A. Lewis and R. D. Aines, Encapsulated Liquid Sorbents for Carbon Dioxide Capture, *Nat. Commun.*, 2015, **6**(1), 6124, DOI: 10.1038/ncomms7124.

28 N. Hussain Solangi, F. Hussin, A. Anjum, N. Sabzoi, S. Ali Mazari, N. M. Mubarak, M. Kheireddine Aroua, M. T. H. Siddiqui and S. Saeed Qureshi, A Review of Encapsulated Ionic Liquids for CO2 Capture, *J. Mol. Liq.*, 2023, **374**, 121266, DOI: 10.1016/j.molliq.2023.121266.

29 L. Al-Mahbobi, A. Klemm, C. Taylor, B. Gurkan and E. Pentzer, CO $_2$ Capture with Capsules of Ionic Liquid/Amines, *ACS Appl. Eng. Mater.*, 2024, **2**(5), 1298–1305, DOI: 10.1021/acsaenm.4c00118.

30 J. K. Stolaroff, C. Ye, J. S. Oakdale, S. E. Baker, W. L. Smith, D. T. Nguyen, C. M. Spadaccini and R. D. Aines, Microencapsulation of Advanced Solvents for Carbon Capture, *Faraday Discuss.*, 2016, **192**, 271–281, DOI: 10.1039/C6FD00049E.

31 J. K. Stolaroff, C. Ye, D. T. Nguyen, J. Oakdale, J. M. Knipe and S. E. Baker, CO2 Absorption Kinetics of Micro-Encapsulated Ionic Liquids, *Energy Procedia*, 2017, **114**, 860–865, DOI: 10.1016/j.egypro.2017.03.1228.

32 S. Kaviani, S. Kolahchyan, K. L. Hickenbottom, A. M. Lopez and S. Nejati, Enhanced Solubility of Carbon Dioxide for Encapsulated Ionic Liquids in Polymeric Materials, *Chem. Eng. J.*, 2018, **354**, 753–757, DOI: 10.1016/j.cej.2018.08.086.

33 B. Rodier, A. De Leon, C. Hemmingsen and E. Pentzer, Controlling Oil-in-Oil Pickering-Type Emulsions Using 2D Materials as Surfactant, *ACS Macro Lett.*, 2017, **6**(11), 1201–1206, DOI: 10.1021/acsmacrolett.7b00648.

34 Q. Luo, Y. Wang, Z. Chen, P. Wei, E. Yoo and E. Pentzer, Pickering Emulsion-Templated Encapsulation of Ionic Liquids for Contaminant Removal, *ACS Appl. Mater. Interfaces*, 2019, **11**(9), 9612–9620, DOI: 10.1021/acsami.8b21881.

35 K. Edgehouse, N. Starvaggi, N. Rosenfeld, D. Bergbreiter and E. Pentzer, Impact of Shell Composition on Dye Uptake by Capsules of Ionic Liquid, *Langmuir*, 2022, **38**(45), 13849–13856, DOI: 10.1021/acs.langmuir.2c02015.

36 Q. Luo and E. Pentzer, Encapsulation of Ionic Liquids for Tailored Applications, *ACS Appl. Mater. Interfaces*, 2020, **12**(5), 5169–5176, DOI: 10.1021/acsami.9b16546.

37 Q. Huang, Q. Luo, Y. Wang, E. Pentzer and B. Gurkan, Hybrid Ionic Liquid Capsules for Rapid CO $_2$ Capture, *Ind.*

Eng. Chem. Res., 2019, **58**(24), 10503–10509, DOI: 10.1021/acs.iecr.9b00314.

38 N. C. Starvaggi, B. J. Bradford, C. D. L. Taylor and E. B. Pentzer, Wettability-Tuned Silica Particles for Emulsion-Templated Microcapsules, *Soft Matter*, 2023, **19**(39), 7635–7643, DOI: 10.1039/D3SM00860F.

39 S. S. Gaur, K. J. Edgehouse, A. Klemm, P. Wei, B. Gurkan and E. B. Pentzer, Capsules with Polyurea Shells and Ionic Liquid Cores for CO_2 Capture, *J. Polym. Sci.*, 2021, **59**(23), 2980–2989, DOI: 10.1002/pol.20210342.

40 Y.-Y. Lee, K. Edgehouse, A. Klemm, H. Mao, E. Pentzer and B. Gurkan, Capsules of Reactive Ionic Liquids for Selective Capture of Carbon Dioxide at Low Concentrations, *ACS Appl. Mater. Interfaces*, 2020, **12**(16), 19184–19193, DOI: 10.1021/acsami.0c01622.

41 C. D. L. Taylor, A. Klemm, L. Al-Mahbobi, B. J. Bradford, B. Gurkan and E. B. Pentzer, Ionic Liquid–Glycol Mixtures for Direct Air Capture of CO_2 : Decreased Viscosity and Mitigation of Evaporation *Via* Encapsulation, *ACS Sustain. Chem. Eng.*, 2024, **12**(20), 7882–7893, DOI: 10.1021/acssuschemeng.4c01265.

42 N. C. Starvaggi, L. Al-Mahbobi, M. Zeeshan, E. C. Barrios, B. Gurkan and E. B. Pentzer, Double Emulsion Microencapsulation of Ionic Liquids for Carbon Capture, *Mater. Horiz.*, 2024, **11**(23), 6057–6063, DOI: 10.1039/D4MH00796D.

43 G. Firpo, E. Angeli, L. Repetto and U. Valbusa, Permeability Thickness Dependence of Polydimethylsiloxane (PDMS) Membranes, *J. Membr. Sci.*, 2015, **481**, 1–8, DOI: 10.1016/j.memsci.2014.12.043.

44 K. Berean, J. Z. Ou, M. Nour, K. Latham, C. McSweeney, D. Paull, A. Halim, S. Kentish, C. M. Doherty, A. J. Hill and K. Kalantar-zadeh, The Effect of Crosslinking Temperature on the Permeability of PDMS Membranes: Evidence of Extraordinary CO2 and CH4 Gas Permeation, *Sep. Purif. Technol.*, 2014, **122**, 96–104, DOI: 10.1016/j.seppur.2013.11.006.

45 Z. Zhu, N. Kumar, U. I. Premadasa, J. T. Damron, D. Stamberga, N. Oldham, Y.-Z. Ma, R. Custelcean, V. S. Bryantsev, B. Doughty, S. Roy and V. Bocharova, Polymer Layer-Accelerated CO_2 Absorption in Aqueous Amino Acid Solutions, *ACS Appl. Polym. Mater.*, 2024, acsapm.4c02798, DOI: 10.1021/acsapm.4c02798.

46 A. Vaishnav, S. Fujikawa and A. Staykov, Curvature Effect in Polydimethylsiloxane Interaction with CO_2, Insights from Theory, *J. Phys. Chem. A*, 2023, **127**(4), 876–885, DOI: 10.1021/acs.jpca.2c07001.

47 G. Rim, T. G. Feric, T. Moore and A. A. Park, Solvent Impregnated Polymers Loaded with Liquid-Like Nanoparticle Organic Hybrid Materials for Enhanced Kinetics of Direct Air Capture and Point Source CO_2 Capture, *Adv. Funct. Mater.*, 2021, **31**(21), 2010047, DOI: 10.1002/adfm.202010047.

48 J. E. Rainbolt, P. K. Koech, C. R. Yonker, F. Zheng, D. Main, M. L. Weaver, J. C. Linehan and D. J. Heldebrant, Anhydrous Tertiary Alkanolamines as Hybrid Chemical and Physical CO_2 Capture Reagents with Pressure-Swing Regeneration, *Energy Env. Sci*, 2011, **4**(2), 480–484, DOI: 10.1039/C0EE00506A.

49 W. Wang, X. Zhang, J. Liu, C. Liang, J. Niu and F. Wang, Review of Moisture Swing Sorbents for Carbon Dioxide Capture from Ambient Air, *Int. J. Glob. Warm.*, 2024, **32**(2), 119–147, DOI: 10.1504/IJGW.2024.135979.

50 B. M. Balasubramaniam, P.-T. Thierry, S. Lethier, V. Pugnet, P. Llewellyn and A. Rajendran, Process-Performance of Solid Sorbents for Direct Air Capture (DAC) of CO2 in Optimized Temperature-Vacuum Swing Adsorption (TVSA) Cycles, *Chem. Eng. J.*, 2024, **485**, 149568, DOI: 10.1016/j.cej.2024.149568.

51 R. Sharifian, R. M. Wagterveld, I. A. Digdaya, C. Xiang and D. A. Vermaas, Electrochemical Carbon Dioxide Capture to Close the Carbon Cycle, *Energy Environ. Sci.*, 2021, **14**(2), 781–814, DOI: 10.1039/D0EE03382K.

52 M. Zeeshan, A. Klemm, J. T. Damron, K. A. Unocic, M. K. Kidder and B. Gurkan, Ionic Liquid Functionalizes the Metal Organic Framework for Microwave-Assisted Direct Air Capture of CO_2, *ACS Mater. Lett.*, 2024, **6**(8), 3854–3861, DOI: 10.1021/acsmaterialslett.4c00804.

53 R. Boylu, M. Erguvan and S. Amini, Investigation of Microwave-Based CO2 Regeneration in a Packed Bed Reactor for Direct Air Capture, *Chem. Eng. Res. Des.*, 2024, **212**, 391–404, DOI: 10.1016/j.cherd.2024.11.014.

54 P. Amornsin, P. Nokpho, X. Wang, P. Piumsomboon and B. Chalermsinsuwan, Investigation of Microwave-Assisted Regeneration of Zeolite 13X for Efficient Direct Air CO2 Capture: A Comparison with Conventional Heating Method, *Sci. Rep.*, 2025, **15**(1), 18376, DOI: 10.1038/s41598-025-02074-z.

55 D. Bermudez-Aguirre and B. A. Niemira, Radio Frequency Treatment of Food: A Review on Pasteurization and Disinfestation, *Foods*, 2023, **12**(16), 3057, DOI: 10.3390/foods12163057.

56 J. H. Oh, A. D. Martinez, H. Cao, G. W. George, J. S. Cobb, P. Sharma, L. A. Fassero, K. Arole, M. A. Carr, K. M. Lovell, J. Shukla, M. A. Saed, R. Tandon, M. E. Marquart, L. C. Moores and M. J. Green, Radio Frequency Heating of Washable Conductive Textiles for Bacteria and Virus Inactivation, *ACS Appl. Mater. Interfaces*, 2022, **14**(38), 43732–43740, DOI: 10.1021/acsami.2c11493.

57 S. Tsubaki, K. Furusawa, H. Yamada, T. Kato, T. Higashii, S. Fujii and Y. Wada, Insights into the Dielectric-Heating-Enhanced Regeneration of CO_2 -Rich Aqueous Amine Solutions, *ACS Sustain. Chem. Eng.*, 2020, **8**(36), 13593–13599, DOI: 10.1021/acssuschemeng.0c05342.

58 C.-M. Hsieh, L. Al-Mahbobi, S. S. Dasari, M. Avais, H. Cao, P. Wei, Y. Wang, M. J. Green and E. B. Pentzer, Fusion of Capsules to Produce Liquid-Filled Monoliths for Carbon Capture, *J. Mater. Chem. A*, 2024, **12**(43), 29749–29762, DOI: 10.1039/D4TA04906C.

59 M. Anas, M. M. Mustafa, A. Vashisth, E. Barnes, M. A. Saed, L. C. Moores and M. J. Green, Universal Patterns of Radio-Frequency Heating in Nanomaterial-Loaded Structures, *Appl. Mater. Today*, 2021, **23**, 101044, DOI: 10.1016/j.apmt.2021.101044.

60 S. S. Dasari, A. Sarmah, R. D. Mee, A. N. Khalfaoui and M. J. Green, Joule Heating of Carbon Fibers and Their Composites in Radio-Frequency Fields, *Adv. Eng. Mater.*, 2023, **25**(10), 2201631, DOI: 10.1002/adem.202201631.

61 Y. Lee, E. Cagli, A. Klemm, Y. Park, R. Dikki, M. K. Kidder and B. Gurkan, Microwave Regeneration and Thermal and Oxidative Stability of Imidazolium Cyanopyrrolide Ionic Liquid for Direct Air Capture of Carbon Dioxide, *ChemSusChem*, 2023, **16**(13), e202300118, DOI: 10.1002/cssc.202300118.

62 S. Seo, M. A. DeSilva and J. F. Brennecke, Physical Properties and CO_2 Reaction Pathway of 1-Ethyl-3-Methylimidazolium Ionic Liquids with Aprotic Heterocyclic Anions, *J. Phys. Chem. B*, 2014, **118**(51), 14870–14879, DOI: 10.1021/jp509583c.

63 S. Oh, O. Morales-Collazo and J. F. Brennecke, Cation–Anion Interactions in 1-Ethyl-3-Methylimidazolium-Based Ionic Liquids with Aprotic Heterocyclic Anions (AHAs), *J. Phys. Chem. B*, 2019, **123**(39), 8274–8284, DOI: 10.1021/acs.jpcb.9b06102.

64 G. M. Avelar Bonilla, O. Morales-Collazo and J. F. Brennecke, Effect of Water on CO_2 Capture by Aprotic Heterocyclic Anion (AHA) Ionic Liquids, *ACS Sustain. Chem. Eng.*, 2019, **7**(19), 16858–16869, DOI: 10.1021/acssuschemeng.9b04424.

65 G. K. Fleming and W. J. Koros, Dilation of Polymers by Sorption of Carbon Dioxide at Elevated Pressures. 1. Silicone Rubber and Unconditioned Polycarbonate, *Macromolecules*, 1986, **19**(8), 2285–2291, DOI: 10.1021/ma00162a030.

66 J. D. Wind, S. M. Sirard, D. R. Paul, P. F. Green, K. P. Johnston and W. J. Koros, Carbon Dioxide-Induced Plasticization of Polyimide Membranes: Pseudo-Equilibrium Relationships of Diffusion, Sorption, and Swelling, *Macromolecules*, 2003, **36**(17), 6433–6441, DOI: 10.1021/ma0343582.

67 M. Sadrzadeh, K. Shahidi and T. Mohammadi, Synthesis and Gas Permeation Properties of a Single Layer PDMS Membrane, *J. Appl. Polym. Sci.*, 2010, **117**(1), 33–48, DOI: 10.1002/app.31180.

68 R. Swaidan, B. Ghanem, M. Al-Saeedi, E. Litwiller and I. Pinnau, Role of Intrachain Rigidity in the Plasticization of Intrinsically Microporous Triptycene-Based Polyimide Membranes in Mixed-Gas CO_2/CH_4 Separations, *Macromolecules*, 2014, **47**(21), 7453–7462, DOI: 10.1021/ma501798v.

69 J. E. Bachman, Z. P. Smith, T. Li, T. Xu and J. R. Long, Enhanced Ethylene Separation and Plasticization Resistance in Polymer Membranes Incorporating Metal–Organic Framework Nanocrystals, *Nat. Mater.*, 2016, **15**(8), 845–849, DOI: 10.1038/nmat4621.

70 F. Raganati, M. Alfe, V. Gargiulo, R. Chirone and P. Ammendola, Kinetic Study and Breakthrough Analysis of the Hybrid Physical/Chemical CO2 Adsorption/Desorption Behavior of a Magnetite-Based Sorbent, *Chem. Eng. J.*, 2019, **372**, 526–535, DOI: 10.1016/j.cej.2019.04.165.

71 G. Romanos, L. M. Pastrana-Martínez, T. Tsoufis, C. Athanasekou, E. Galata, F. Katsaros, E. Favvas, K. G. Beltsios, E. Siranidi, P. Falaras, V. Psycharis and A. M. T. Silva, A Facile Approach for the Development of Fine-Tuned Self-Standing Graphene Oxide Membranes and Their Gas and Vapor Separation Performance, *J. Membr. Sci.*, 2015, **493**, 734–747, DOI: 10.1016/j.memsci.2015.07.034.

72 Y. Dai, X. Ruan, Z. Yan, K. Yang, M. Yu, H. Li, W. Zhao and G. He, Imidazole Functionalized Graphene Oxide/PEBAX Mixed Matrix Membranes for Efficient CO2 Capture, *Sep. Purif. Technol.*, 2016, **166**, 171–180, DOI: 10.1016/j.seppur.2016.04.038.

73 D. Chen, L. Li, R. Semiat and X. He, Process Parametric Investigation of Graphene-Oxide-Embedded Composite Membranes for Boosting CO_2/N_2 Separation, *Energy Fuels*, 2023, **37**(15), 11187–11196, DOI: 10.1021/acs.energyfuels.3c01927.

74 B. Gurkan and M. Zeeshan, *Sorbent Regeneration via Radio Frequency Assisted Dielectric Heating for Direct Air Capture of CO_2*, 2024, DOI: 10.26434/chemrxiv-2024-xwfsc.

75 L. Qiu, L. Peng, D. Moitra, H. Liu, Y. Fu, Z. Dong, W. Hu, M. Lei, D. Jiang, H. Lin, J. Hu, K. A. McGarry, I. Popovs, M. Li, A. S. Ivanov, Z. Yang and S. Dai, Harnessing the Hybridization of a Metal-Organic Framework and Superbase-Derived Ionic Liquid for High-Performance Direct Air Capture of CO2, *Small*, 2023, **19**(41), 2302708, DOI: 10.1002/smll.202302708.

76 S. Mukherjee, N. Sikdar, D. O'Nolan, D. M. Franz, V. Gascón, A. Kumar, N. Kumar, H. S. Scott, D. G. Madden, P. E. Kruger, B. Space and M. J. Zaworotko, Trace CO_2 Capture by an Ultramicroporous Physisorbent with Low Water Affinity, *Sci. Adv.*, 2019, **5**(11), eaax9171, DOI: 10.1126/sciadv.aax9171.

77 F. Su and C. Lu, CO2 Capture from Gas Stream by Zeolite 13X Using a Dual-Column Temperature/Vacuum Swing Adsorption, *Energy Environ. Sci.*, 2012, **5**(10), 9021, DOI: 10.1039/c2ee22647b.